Fully Coupled Inversion on a Multi-Physical Reservoir Model - Part II: The Ketzin CO$_2$ storage reservoir

Florian M. Wagner[b,1], Bernd U. Wiese[a,*]

[a]*GFZ German Research Centre for Geosciences, Section 6.3 Geological Storage, Potsdam, Germany*
[b]*University of Bonn, Steinmann Institute, Department of Geophysics, Bonn, Germany*
[c]*ETH Zurich, Institute of Geophysics, Zurich, Switzerland*

Abstract

Reliable monitoring of CO$_2$ storage reservoirs requires a combination of different observation methods. However, history matching is typically limited to CO$_2$ pressure data alone. This paper presents a multi-physical inversion of hydraulic pressure, CO$_2$ pressure, CO$_2$ arrival time and geoelectrical crosshole observations of the Ketzin pilot site for CO$_2$ storage, Germany. Multi-physical inversion has rarely been reported for CO$_2$ storage reservoirs. In contrast to previous studies, there is no need for pre-inversion of geophysical datasets as these are now directly included in a fully coupled manner. The deteriorating impact of structural noise is effectively mitigated by preconditioning of the observation data. A double regularisation scheme provides stability for insensitive parameters and reduces the number of required model runs during inversion. The model shows fast and stable convergence and the results provide a good fit to the multi-physical observation dataset. It has certain predictive power as the known migration direction of the CO$_2$ plume is captured. These results clarify two long discussed issues of the Ketzin CO$_2$ storage reservoir: 1) The pre-existing hypothesis of an existing hydraulic barrier became unsubstantial as the data series suggesting weak hydraulic communication are identified as erroneous. 2) Salt precipitation around the injection well doubles the injection overpressure compared to salt free conditions, which is equivalent to a well skin of 10. The presented framework allows to integrate various types of observations into a single multi-physical model leading to an increased confidence in the spatial permeability distribution and, in perspective, to improved predictive assessments of CO$_2$ storage reservoirs.

Keywords: Multi-physical, Hydrogeophysical, Inverse reservoir modeling, Pumping tests, Pressure, Geoelectrical monitoring, Barrier, Salt precipitation, CO$_2$ storage, Ketzin

1. Introduction

The Ketzin pilot site is Europe's longest operating onshore CO$_2$ storage site geologically located within the North-East German Basin about 25 km west of Berlin. Between June 2008 and August 2013, approximately 67 kt of CO$_2$ have been stored within the Stuttgart Formation, a sandstone of the Upper Triassic (Martens et al., 2014). Numerical simulations of CO$_2$ migration have been an integral component during all stages of the storage operation. Based on an initial geological model (Förster et al., 2006), Kempka et al. (2010) present a history match of the CO$_2$ arrival at the first observation well. Lengler et al. (2010) investigate the impact of unknown spatial heterogeneity

by means of a stochastic Monte Carlo approach. Based on a revised geological model (Norden and Frykman, 2013), Kempka and Kühn (2013) use near-well and far-well permeability multipliers to manually history match a revised flow model that is in agreement with long-term pressure measurements and observed arrival times, but does not capture high magnitude short-term pressure variations. Disregarding observation data is commonly the cost of manual model calibration (e.g. Oliver and Chen, 2010).

Class et al. (2015) present the first automated calibration of Ketzin reservoir models based on a small number of parameters. Yet their calibration is solely based on pressure and arrival time data and does not include geophysical measurements with a larger spatial resolution. Lüth et al. (2015) recently assessed the conformity between large-scale 4D seismic data and a manually history-matched reservoir model considering several performance

---

*Corresponding author: Bernd U. Wiese

Email address: wiese@gfz-potsdam.de (Bernd U. Wiese)
[1]Previously at [a] and [c]

criteria such as the footprint, volume, and lateral migration distance of the CO_2, as well as a similarity index to quantify the areal overlap between observed and simulated plumes. The authors discuss uncertainties in both monitoring and simulation results and demonstrate a reasonable conformance between the observed and simulated plume behaviour under consideration of the relatively high noise level inherent for land-based geophysical monitoring data.

The test site was also characterised with hydraulic simulations based on three cross hole pumping tests, which were conducted prior to CO_2 injection. The traditional form of analysing each of the nine time series analytically results in significant ambiguity and at least three different conceptual models, as discussed by Wiese et al. (2010). Chen et al. (2014) and Kempka and Norden (2017) use the data in an inverse modelling framework to estimate a near-well permeability distribution. The authors state the hypothesis of a large barrier zone between injection well Ktzi201 and observation wells Ktzi200 and Ktzi202 and as consequence strongly channeled flow inbetween, but conclude that only limited information at the inter-well scale can be extracted from the pumping test data. The standalone geoelectrical inversions provide certain support for the barrier hypothesis, but information remains ambiguous (Schmidt-Hattenberger et al., 2011, 2012; Bergmann et al., 2017). Chen et al. (2014) suggest a joint inversion of hydraulic and CO_2 injection data to achieve a better characterisation of the subsurface.

In this study, a CO_2 migration and a hydraulic model of the Ketzin reservoir are combined and constrained by multi-physical observations. Based on a recently developed inversion approach (Wiese et al., 2018, this issue), the hydraulic data is supplemented with reservoir pressure, CO_2 arrival times and geoelectrical crosshole data in order to decrease the ambiguity and to better characterise the subsurface heterogeneity at the site. Fully coupled inversion of these types of field observations has not been reported before and aims to close that gap to allow answering questions which could not be addressed with previous Ketzin models. This paper aims to integrate hydraulic tests and CO_2 injection time series quantitavely to determine relative permeability components and aims to clarify the unexpectedly weak hydraulic communication between two wells at the Ketzin test site that was interpreted as hydraulic barrier in previous studies (Wiese et al., 2010; Chen et al., 2014). Salt precipitation is modelled by e.g. ?Pruess and Müller (2009) and experimentally shown by Bacci et al. (2011); Jeddizahed and Rostami (2016) to reduce injection well permeability. It is known to occur in the Ketzin injection well (Baumann et al., 2014) but its effect could not be distinguished from intrinsic permeability in previous Ketzin reservoir models. The present approach aims to constrain the plume shape from geoelectrical data measured in all three wells at the site. Previous classical tomographic inversions of geoelectrical data did not include data of observation well Ktzi202 due to connection loss to the seven lowermost electrodes and the resulting low coverage.

The geoelectrical data are linked to CO_2 saturation with the geoelectrical saturation exponent (Eq. 3 in Wiese et al., 2018, this issue). For a Ketzin sample Kummerow and Spangenberg (2011) determined a value of 1.62. Within this study, a further experiment is carried out. These results are used as the range for calibrating a homogeneous saturation exponent for the Ketzin test site.

This case study aims at a comprehensive interpretation of the multi-physical Ketzin dataset to achieve a better quantification of the reservoir and injection processes.

2. Multi-physical monitoring and characterisation

Geological storage activities at Ketzin are accompanied by a comprehensive monitoring program (Köhler et al., 2013). An overview of the applied methods and conducted field campaigns can be found in Martens et al. (2014). For an in-depth summary of all geophysical monitoring activities, the reader is referred to the recent review by Bergmann et al. (2016). Here, the focus lies on monitoring activities relevant for the coupled inversion presented.

2.1. Hydraulic crosshole tests

2.1.1. Data acquisition

Prior to the CO_2 injection, between September 2007 and January 2008, pumping tests were conducted as open hole tests in each well while reservoir pressure was observed in all three wells. The tests followed multiple objectives including the removal of residual drilling fluids, production of formation water samples, identification of near-well conditions, as well as the estimation of field-scale permeability (Wiese et al., 2010). Under consideration of the maximum allowable drawdown, pumping rates ranged between 1.1 and 1.8 m^3/h (Wiese et al., 2010).

2.1.2. Data filtering and pre-processing

For efficient computing, similar pumping rates are averaged over the corresponding periods and simulated pressures are generated for the end of each of these periods. Pressure data observations are chosen accordingly. For

pumping tests in wells Ktzi200 and Ktzi202 the undisturbed initial pressure level is known. For the pumping test in well Ktzi201 first observations are available after pumping started, wherefore the reference level is approximated with the highest pressure in the respective well during the test. The simulated data are processed accordingly.

The hydraulic dataset consists of time series, each representing a pumping well - observation well combination. Chen et al. (2014) could not achieve a satisfying model fit for observation in Ktzi200 with pumping in Ktzi201, but could not discriminate whether it is a data error or a local heterogeneity. Also with the present model it is not possible to find a permeability field when including both time series referring to the cross hole combination of wells Ktzi200 and Ktzi201. By elimination of just one of these time series a satisfying fit of the observed data could be obtained, but at the cost of a very heterogeneous permeability field with values frequently hitting parameter bounds at 1 and 1000 mD, which is a severe sign for overfitting, i.e. either fitting data too well subject to model simplifications with respect to reality or fitting of corrupted data. Both erroneous pumping tests have been carried out subsequently by interchanging pump and logger between the wells. A defective pressure logger would corrupt both time series. Therefore, both time series are not included in the further calibration.

2.2. CO$_2$ monitoring

2.2.1. Data acquisition

The mass flux of the injection stream and the reservoir pressure have been monitored continuously in five second intervals in the injection well Ktzi201. The actual flow rate of CO$_2$, measured within the injection pipeline 8 m upstream of the injection well (Liebscher et al., 2013), serves as an input to the CO$_2$ model, whereas reservoir pressure and arrival times serve as observation data to the inversion. Reservoir pressure is vital for model calibration and a good match between measured and modelled values is considered to be the most important prerequisite for predictive assessments (e.g. Class et al., 2015). In the presented inversion framework, the observed pressure of the injection well Ktzi201 is therefore included, which was measured with a pressure-temperature point gauge based on two Fiber-Bragg gratings at the end of the injection tubing at 550 m depth (Liebscher et al., 2013). Arrival times of CO$_2$ were monitored at both observation wells (Ktzi200 and Ktzi202) with a gas membrane sensor (Zimmer et al., 2011) and wellhead pressure.

2.2.2. Data filtering and pre-processing

To ensure efficiency and integrity of the simulations, injection is averaged over periods with similar CO$_2$ rates and simulated values are generated for the end of each of these periods. Pressure sensor data are chosen accordingly. To increase inversion stability, short and long term pressure differences are calibrated instead of direct values (Wiese et al., 2018, this issue).

The reservoir pressure is calculated by correction of the sensor data for the static gas column to the reference depth of 640 m since friction losses and inertial effects can be neglected (Wiese et al., 2012). Arrival times are defined when the gaseous CO$_2$ saturation of at least one model cell in the respective well has reached 3%.

2.3. Geoelectrical crosshole monitoring

2.3.1. Data acquisition

Crosshole electrical resistivity measurements are conducted on a weekly basis since the beginning of injection in June 2008 (Bergmann et al., 2017). Data acquisition is realised with the aid of a permanently installed vertical electrical resistivity array (VERA) consisting of 45 ring-shaped stainless steel electrodes mounted on the electrically insulated borehole casings of the injection well and the first two observation wells. During data acquisition, an electric current of up to 2.5 A is injected between two current electrodes and a potential measurement, typically in the range of 50 μV to 100 mV, is registered between two observation electrodes. Acquired crosshole configurations include bipole-bipole measurements, where the two electrodes of a bipole are either split across different boreholes (AM-BN; Figure 7) or situated in one borehole (AB-MN). These are supplemented by a limited number of inhole (ABMN) and pole-tripole (A-BMN) measurements (Schmidt-Hattenberger et al., 2011, 2016).

2.3.2. Data filtering and pre-processing

Tomographic studies using geoelectrical data from the Ketzin site have focused on the 2D imaging plane between the injection well Ktzi201 and the first observation well Ktzi200 (Schmidt-Hattenberger et al., 2013; Wagner et al., 2015; Schmidt-Hattenberger et al., 2016). The reason for this is the decreased 3D coverage due to the loss of connection to the seven lowermost electrodes in the observation well Ktzi202. Since this study directly uses the entire time-lapse dataset to estimate hydraulic subsurface properties in the frame of a multi-physical inversion, the need for a classical geoelectrical tomographic inversion is effectively circumvented. We state the hypothesis that a process based inversion can be effectively calibrated with a

lower geoelectrical coverage compared to traditional geo-electrical inversion because the parameter distribution is additionally constrained by geology and the flow model. In consequence, we consider the complete 4D dataset including measurements from wells Ktzi200, Ktzi201, and Ktzi202.

A rigorous filtering procedure is applied on the measured apparent resistivity time series since poor data quality can compromise stability and results of the inversion. Any processing is limited to the 1008 four-point configurations, which have been measured at least once per month exclusively with electrodes known to be intact based on regular contact resistance checks. In addition, any configurations are excluded where no reciprocal counterparts exist for direct error quantification. From this set all configurations that exhibit geometric factors larger than 10^4 m and time-lapse reciprocal errors above 5 % are filtered out. The latter is defined as the root-mean-square deviation between the forward and reciprocal apparent resistivity time series. In a last step, a moving average filter with a time window of two weeks is applied to all time series in order to remove measurement gaps and strongly deviating outliers.

A total number of 226 time series, each measured by an individual electrode configuration, remains for inversion. Daily averages of apparent resistivity are normalized with their respective pre-injection value and used as observations for inversion. The final input dataset consists of 61,698 apparent resistivity ratios (226 time series à 273 days).

It is noteworthy that the described filtering procedure almost completely removes inhole and AB-MN type configurations, which are known to suffer from low signal-to-noise ratios (Bing and Greenhalgh, 2000) and pronounced sensitivity to borehole related effects (Doetsch et al., 2010). In consequence, the calibration is mainly based on AM-BN and a few A-BMN type configurations.

2.3.3. Petrophysical experiments

To link the apparent resistivity ratios to CO_2 saturations, it is assumed that the pore space is filled with a two-phase mixture of brine and CO_2 and that surface conductance, temperature, as well as pressure effects can be neglected (Eq. 3 in Wiese et al., 2018, this issue). In order to constrain the saturation exponent n, laboratory experiments were conducted, during which the electrical resistivity of a reservoir rock sample was measured with increasing brine saturation under ambient conditions.

The sample of reservoir sandstone has a height of 55 mm and a radius of 15 mm and was taken from the injection
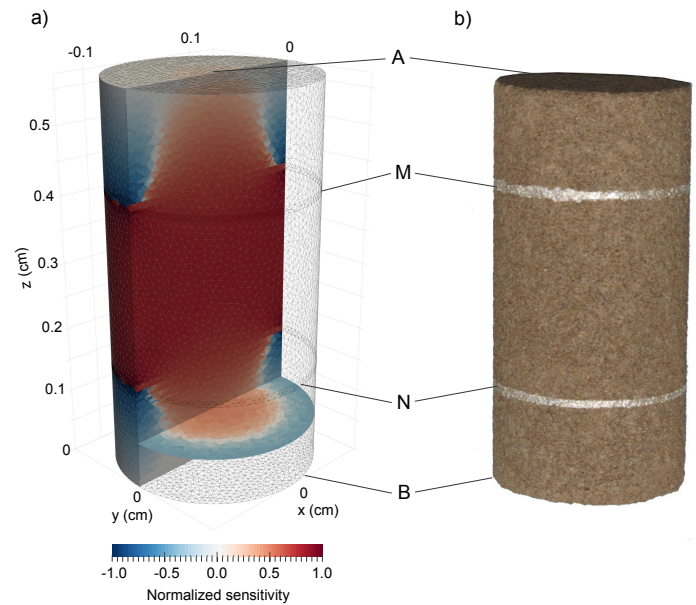
Figure 1: (a) Modelled electrical sensitivity distribution throughout the cylindrical rock sample assuming homogeneity. (b) Photograph of the rock sample showing the two potential electrodes consisting of conductive silver lacquer. A and B mark the current injecting electrodes, whereas M and N mark the electrodes used for potential measurements.

well Ktzi201 at 638 m depth. Brine was repeatedly added to the sample and the saturation was determined under consideration of its actual, dry, and fully saturated mass. Current injection was performed via two metal plates at the top and the bottom of the sample. To acquire potential differences, the sample was prepared with two rings of conductive silver lacquer as shown in Figure 1b.

Figure 1a shows the resulting sensitivity distribution modelled throughout a homogeneous rock sample fully accounting for distributed current injection via plate and ring electrodes based on the complete electrode model (Rücker and Günther, 2011). It can be seen that negative sensitivity develops between A and M and B and N, respectively, while constant positive sensitivity is only obtained between the two potential electrodes M and N. It was therefore crucial to allow time for equilibrium of the injected brine subsequent to the initialisation of a new saturation level in order to obtain representative measurements. Figure 2 shows the measured resistivity of the sample ρ_t divided by its saturated resistivity ρ_0 (at $S_w = 1$) as a function of brine saturation.

The resistivity of the sample decreases with increasing brine saturation with a slope corresponding to $n = 2.6$. Together with other Ketzin specific values previously determined by Kummerow and Spangenberg (2011) of $n = 1.62$ and by Fleury et al. (2013) of n ranging between
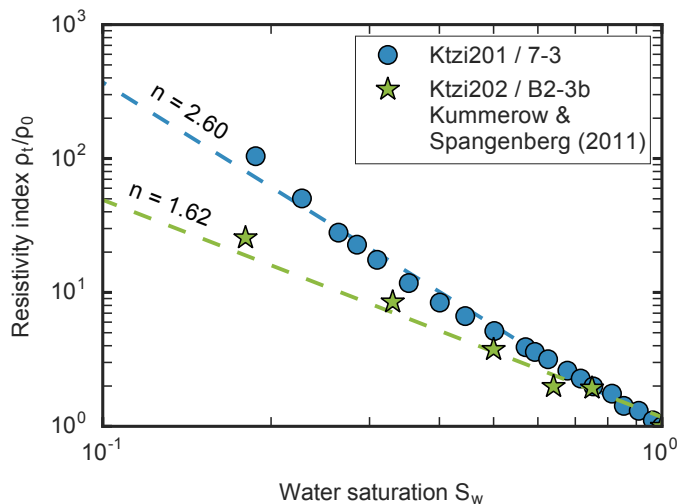
Figure 2: Change in bulk resistivity as a function of water saturation measured for a rock sample from the injection well (Ktzi201) compared to measurements on a sample from the second observation well (Ktzi202) performed by Kummerow and Spangenberg (2011). Dashed lines mark the linear trend where the slope corresponds to the negative saturation exponent.

1.65 and 1.8, the boundaries for the saturation exponent are set to 1.62 and 2.6. These values cover the entire typical range of the saturation exponent for sandstone between 1.6 and 2.6 (Tiab and Donaldson, 2016). This reflects the high level of heterogeneity within the reservoir. Kummerow and Spangenberg (2011) attribute the comparably small value of the saturation exponent to the high clay content of the sample.

3. Inversion approach

The multi-physical field observations are used to estimate reservoir permeability by means of a recently developed fully coupled inversion approach. For details the reader is referred to Wiese et al. (2018, this issue). Here, adaptions necessary for application to the Ketzin field dataset are discussed.

Compared to synthetically generated observations, field data quality is typically lower and data may contain measurement errors such as stochastic noise, hysteresis, data logger drift and even potentially explicit errors. Structural noise is introduced by conceptual simplification (Doherty and Welter, 2010). In comparison to the synthetic case study presented in Wiese et al. (2018, this issue), more flexibility to the relative permeability is given by calibrating the endpoint for full saturation of a specific phase (constant C_i in Eq. 1 in Wiese et al., 2018, this issue). Furthermore, a skin factor is introduced to the CO_2 mi-

gration model as a means to represent diverging behaviour between the hydraulic and the multiphase model.

Calibration of petrophysical parameters is also carried out during coupling of the geoelectrical model. As previously discussed, petrophysical experiments revealed considerable heterogeneity in the saturation exponent. Therefore, the saturation exponent (n in Eq. 3 in Wiese et al., 2018, this issue) is included as a free calibration parameter and varied between 1.62 and 2.6 based on the petrophysical experiments conducted (Figure 2). While this adds additional flexibility, the assumption of a spatially (and temporally) constant saturation exponent throughout the entire reservoir remains.

4. Results and discussion

4.1. Calibrated model parameters

4.1.1. Permeability distribution

The estimated permeability distribution within the sandstone layers of the model is shown in Figure 3. The layers correspond to the conceptual geological model presented by Wiese et al. (2018, this issue, Fig. 2).

The inversion results clearly indicate near-well heterogeneities in the permeability distribution necessary to explain the observation data. Layers that are expected to play a minor role on CO_2 migration have less complex permeability structures (layers 3 & 4).

It was hypothesised that a hydraulic barrier exisits between the wells Ktzi200 and Ktzi201 (Wiese et al., 2010; Chen et al., 2014). The hypothesis was mainly based on two time series from the pre-injection crosshole pumping tests, which showed low hydraulic communication between Ktzi200 and Ktzi201. These series are identified as erroneous during pretreatment of hydraulic data and therefore eliminated. The inversion of the remaining multiphysical dataset does not show any indication for a hydraulic barrier. A synthetic model with a barrier in layer 1, which is subject to identical operational conditions and measurements, was inverted by Wiese et al. (2018, this issue). The inversion, although carried out under very favourable conditions, only produced a weak barrier structure due to the non-uniqueness induced by the multi-layer system. Considering additional uncertainty from e.g. facies distribution, porosity-permeability scattering, and two hydraulic time series being removed as measurement error in the present dataset, a barrier in one layer would probably not be resolved. Therefore no significant arguments supporting the existence of a barrier remain.
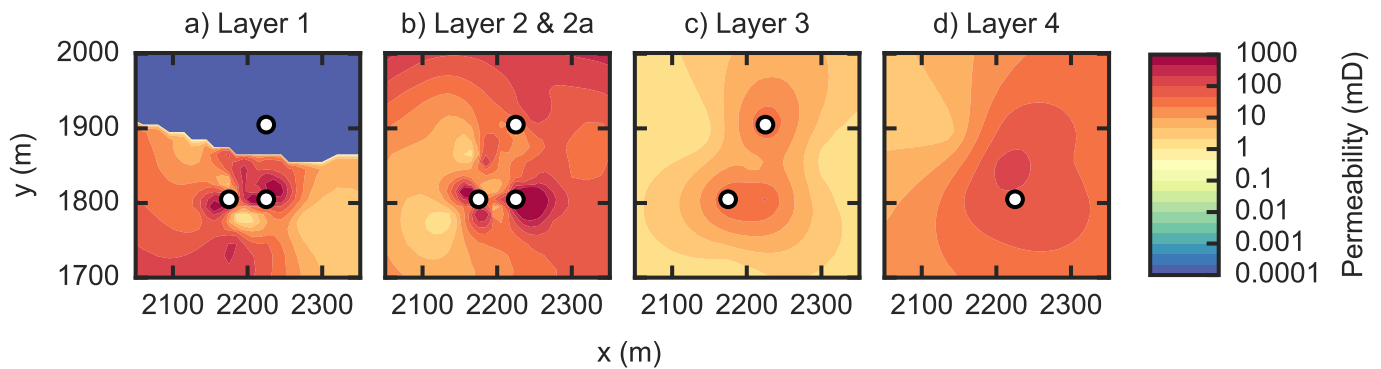
Figure 3: Estimated permeability distribution. Hydraulic connections to wells through screened intervals are indicated by white dots.
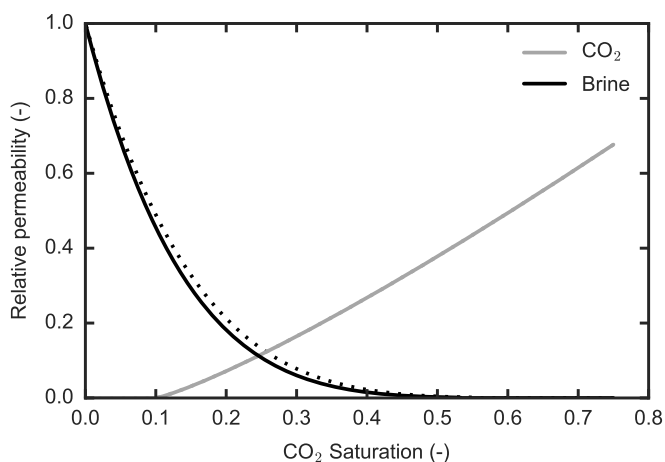
Figure 4: Relative permeability functions for CO_2 (grey) and brine (black). The dotted curves show initial conditions following unpublished Ketzin core measurements, the solid curves show calibrated relative permeabilities. The CO_2 curves match.

4.1.2. Petrophysical parameters

The relative permeability functions for the initial conditions based on laboratory measurements on core samples and after calibration are shown in Figure 4. The calibrated relative permeability function does not deviate significantly from its initial state during the inversion. Earlier inversions showed significant deviations and implausible values in the mixed saturation region. The capability to detect effective ratios between saturated and multiphase permeability is attributed to the simultaneous inversion of pumping tests and CO_2 injection. Single phase hydraulic flow allows a sensitive determination of the intrinsic permeability, while CO_2 injection is additionally sensitive to the relative permeabilities of CO_2 and brine. At the Ketzin test site, the CO_2 injection pressure buildup is about twice as high compared to the intrinsic formation permeability.

As consequence, a skin factor is introduced to the in-

jection well Ktzi201 only for the CO_2 migration model. The skin factor is calibrated to a value of 10.1, which is a considerable value. It causes pressure variations about twice as high compared to a well without skin. This results in realistic relative permeability functions. Two processes that are not captured by the current model could increase the CO_2 injection pressure while not affecting the intrinsic permeability.

Salt precipitation near the injection well, as observed by pulsed neutron-gamma logs (Baumann, 2013), reduces porosity and permeability near the wellbore and would reduce the injectivity of CO_2. It is, however, a complex and dynamic process and the temporally constant skin factor can only be a first approximation to the phenomenon. Permeability reduction by salt precipitation is low at the injection start and increases during ongoing injection (Pruess and Müller, 2009; Bacci et al., 2011). Formation water comes back after an injection stop, dissolves the salt and increases permeability again. A similar effect can be observed in Ketzin where the observed injection pressure shows slower increase compared to simulated injection pressure with a temporally constant skin factor (Figure 6a, beginning of August and October 2008). The observed CO_2 permeability reduction corresponds to a 1 m radius around the injection well with a permeability of about 15 mD, which is a reduction by about factor 8.

Another process leading to discrepancies between hydraulic model and CO_2 migration model may be selective infiltration of CO_2 into layer 1. This would increase the CO_2 velocity in the near well area and therefore the well pressure, similar to a skin effect. The latter hypothesis can be rejected, since the main reservoir layers are saturated with CO_2 and the water table is below the lower end of layer 2 in June 2009 (Baumann et al., 2014). Turbulent (non-Darcy) pressure losses are also rejected as the bottomhole Reynolds number is in the order of 10^{-7}.

The saturation exponent n reached its lower bound ($n = 1.62$) during the calibration. Aside from the strong assumption of a spatially constant saturation exponent, many electrode configurations measure apparent resistivity ratios close to one. These are configurations focussing on the caprock for example, while they have low sensitivity in regions affected by CO_2 migration. This behavior can always be matched by a numerical model with a very low saturation exponent irrespective of the CO_2 migration and the sensitivity pattern of the respective electrode configuration. To cope with the ambiguity in the calibration, it was therefore necessary to constrain the petrophysical parameter calibration to a reasonable range.

4.1.3. Convergence

Convergence of the objective function and the final data misfit improved significantly on the introduction of a skin factor in the injection well. The skin factor allows the model to fit CO_2 injection pressure and hydraulic pressure simultaneously. Before both data series were contradictory to the model, the improvement of hydraulic pressure led to a deterioration of the CO_2 injection pressure. As consequence a valley in the objective function is created. As soon as the trade off is close to optimal, the inversion tends to jump from one side of the valley to the other, deflecting the direction of the solution vector. Through the change of model parameters this induces a more heterogenous parameter field and jumpy behaviour for other model parameters. Convergence also improved after removal of the two contradictory hydraulic data series (subsubsection 2.1.2) with a similar mechanism.

We conclude that poor convergence may be caused by data that is contradictory to the model. It is not relevant whether the model concept is insufficient to resolve physically meaningful data or whether the data are intrinsically contradictory. The relevance of this point increases with the number of different datasets as typically used for multi-physical inversions. When technical reasons for poor convergence can be excluded (Wiese et al., 2018, this issue), convergence behaviour may provide valuable hints on the model concept and the input data.

In the final model setup, convergence was usually achieved after 3-5 iterations. The presented results are from iteration 5, since further iterations led to spurious near-well artifacts with marginal improvements of the observation objective function, which is interpreted as overfitting.

4.2. Observed and simulated data

The individual contributions of each observation data group to the objective function and their relative reduction between the initial and inverted model are listed in Table 1. The model fit can be directly deduced from the objective function of the groups. They are weighted such that the objective function is the square of the average misfit (Wiese et al., 2018, this issue). So for each group a flat line of initial values results in an objective function of 1, an average misfit of 10 %, results in an objective function of 10^{-2}. Only the geoelectrical observation data group is treated in a slightly different way. The weight of the group is reduced by factor 10, because otherwise it dominated the inversion process and deteriorated especially the pressure fit. To compare the fit of the data quality the objective function values have to be multiplied by factor 10.

The observation objective function is reduced by 80 %. Hydraulic, CO_2 pressure, and geoelectrical observations reduce to a data fit between 2×10^{-2} and 4.8×10^{-2}, while the objective function for the arrival times is about one order of magnitude smaller and reduces by 96 %.

4.2.1. Hydraulic pressure

The simulated and observed pressure drawdown is shown in Figure 5. Both series show a very good match, with the largest discrepancies occurring at pump switching for observations made in the respective pumping well. These can be attributed to the cellsize of 5 x 5 m smoothing rapid changes in the pumping rate.

4.2.2. CO_2 arrival

The arrival times show the best fit of all observation data groups with relative deviations of 0.5 and 4 % (Table 2). As the arrival group comprises only two measurements, only two degrees of freedom are required for matching the observations. Numerically, a good match can be obtained much easier.

The measurements bear some uncertainty. Class et al. (2015) emphasise that the observed arrival times at the Ketzin site do not necessarily represent accurate values for the arrival of CO_2 at the well locations, since the gas membrane sensors were located 150 m below the surface. This means that the CO_2 is detected in the moment that bubbles rise in the well. The wellhead pressure increases sharply 1.5 and 3 days after the first detected arrival, respectively. Small accumulation of gaseous CO_2 in the well annulus at earlier times may remain undetected. This uncertainty is compensated by setting the detection threshold to 3 % of gas saturation, corresponding to bubble forming conditions in both wells.

4.2.3. CO_2 pressure

The observed and simulated reservoir pressures in the injection well Ktzi201 are shown in Figure 6. The model

Table 1: Observation objective function components of the individual observation data groups. Relative reduction describes the percentage change between initial and inverted model parameters.

Observation type	Symbol	Initial	Inverted	Relative reduction (%)
Hydraulic	ϕ_{hyd}	5.7×10^{-2}	2×10^{-2}	65
CO_2 arrival	ϕ_{arr}	6.3×10^{-2}	2.4×10^{-3}	96
CO_2 pressure	ϕ_{p}	2.5×10^{-1}	4.8×10^{-2}	81
Geoelectrical	ϕ_{ert}	1.1×10^{-1}	2.5×10^{-2}	77
Sum observation	ϕ_{o}	4.8×10^{-1}	9.4×10^{-2}	80
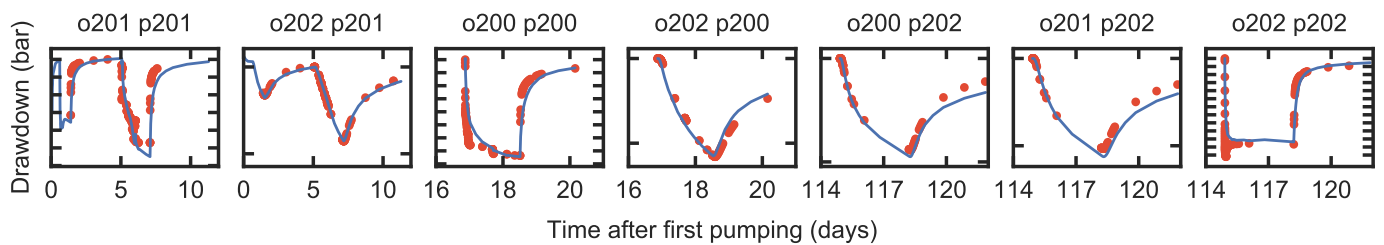
Figure 5: Observed hydraulic drawdown from three cross hole pumping tests and the corresponding model predictions (black curves). Y tick marks have an interval of 1 bar. The first part of the plot title beginning with 'o' denotes to the observation well, the second part beginning with 'p' denotes the pumping well. The series o200 p201 and o201 p200 are not included in the inversion.
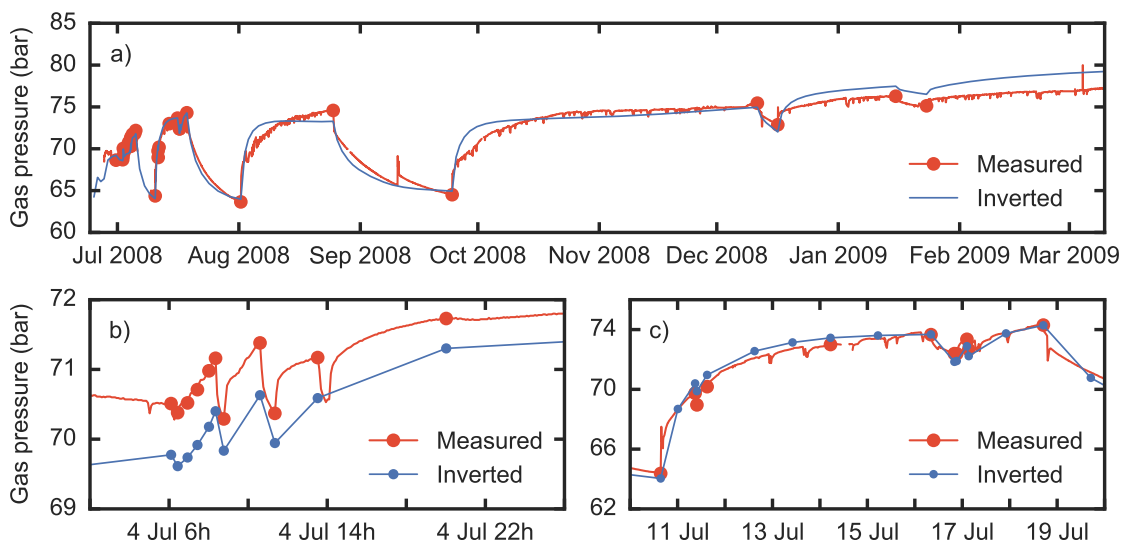
Figure 6: Gas pressure in the injection well Ktzi201. Red dots indicate measured reservoir pressure at the end of a period with constant injection rate and black lines indicate simulated values. Some variability is introduced due to rate variations, illustrated by the red line showing the actual reservoir pressure with a 5 minute interval. Panels b) and c) zoom in to early phases, where the injection rate was varied resulting in short-term pressure differences.

Table 2: Observed and modelled arrival times of gaseous CO_2 at the observation wells.

Observation well	Observed arrival time (days)	Modelled arrival time (days)	Relative deviation (%)
Ktzi200	21.7	21.8	0.5
Ktzi202	271	283	4

shows a good representation of the general trend of the injection pressure. It also shows a very good fit of several short-term changes in injection rate in July 2008 (Figure 6b and Figure 6c). The good fit of the pressure variations at 4th July is remarkable as an offset with the same magnitude exists. Please note that the pressure differences have about twice the magnitude due to salt precipitation (see subsubsection 4.1.2). This represented in a by a simple skin factor. As the real dynamic is not fully captured due to model conceptual simplification (which is necessarily the case for reservoir models) some structural noise is induced. The offset is an example of structural noise and allowed by design due to calibrating pressure differences instead of the direct magnitude. Otherwise a pseudo-fit like a straight line through the respective observations might have occurred.

4.2.4. Geoelectrical observations

The measured and modelled apparent resistivity ratios for selected electrode configurations are shown in Figure 7. The measured apparent resistivity ratios are in good qualitative agreement with the response of the multi-physical model. Most configurations exhibit a continuous increase in apparent resistivity over the investigated time window, such as the AM-BN configuration shown in Figure 7a. However, the quantitative agreement of measured and simulated apparent resistivity ratios is not optimal for all configurations. When comparing the objective function contributions, it has to be considered that the weight is reduced by factor 10.

Figure 7b shows a configuration where one of the electrodes (N) is located directly below the point of injection. While the dynamic behaviour is clearly visible in the early phase in both simulated and measured apparent resistivity curves, their relationship is not satisfactorily described in a quantitative manner. In addition to the inherent simplifications of Archie's Law, this is attributed to the relatively strong assumption of a spatially constant saturation exponent. This saturation exponent is based on petrophysical experiments, which were performed under ambient conditions and may vary under in-situ pressure and temperature and is shown to vary locally between 1.6 and 2.6 (Kummerow and Spangenberg, 2011) (subsubsection 2.3.3). Fluid dynamics in the well annulus change the electrical conditions close to the electrodes and are also known to affect the crosshole measurements (Wagner et al., 2015) and are not captured in the current model.

4.3. Plume migration

The simulated CO_2 plume shape is shown in Figure 8. The CO_2 volume is vertically integrated over all reservoir layers.

Starting at the point of injection, the modelled CO_2 plume exhibits a main migration direction towards the North-West and towards the South. This is in agreement with the migration direction inferred from seismic and surface-downhole geoelectrical monitoring (Bergmann et al., 2016) and not unlikely due to the pronounced heterogeneity of the reservoir. Seismic observations alone indicate that the main migration direction is towards west (Ivandic et al., 2012). This generally correct direction of CO_2 migration is considered as a certain predictive capacity of the model.

5. Conclusions

The applied multi-physical modelling framework integrates a hydraulic model, a multiphase model and a process-based geoelectrical model. The model is calibrated to four types of observation data; hydraulic pressure, CO_2 pressure, CO_2 arrival times and time-lapse electrical resistivity measurements. Since the multi-physical model is inverted in a fully coupled manner, the need for pre-inversion of data subsets, e.g. geoelectrical crosshole data, is circumvented. The data pretreament cancels out structural noise and allows meaningful calibration in spite of an imperfect model fit. The double regularisation scheme allows for overparameterisation as it cancels out the deteriorating effect of insensitive parmeters and reduces the number of required model runs during inversion. The present field study demonstrates the feasibility of our conceptual approach in application to a real world reservoir.

The model shows fast and stable convergence and the field data is well calibrated. The relative permeability functions are calibrated for field conditions. The crosshole ERT data was fully exploited in a quantitative manner as the entire dataset serves as inversion input to estimate reservoir permeability. An effective spatial regularisation is introduced by the reservoir model to allow for inversion of sparse geoelectrical measurements from observation well Ktzi202 for the first time. An effective temporal regularisation is introduced to the daily measured
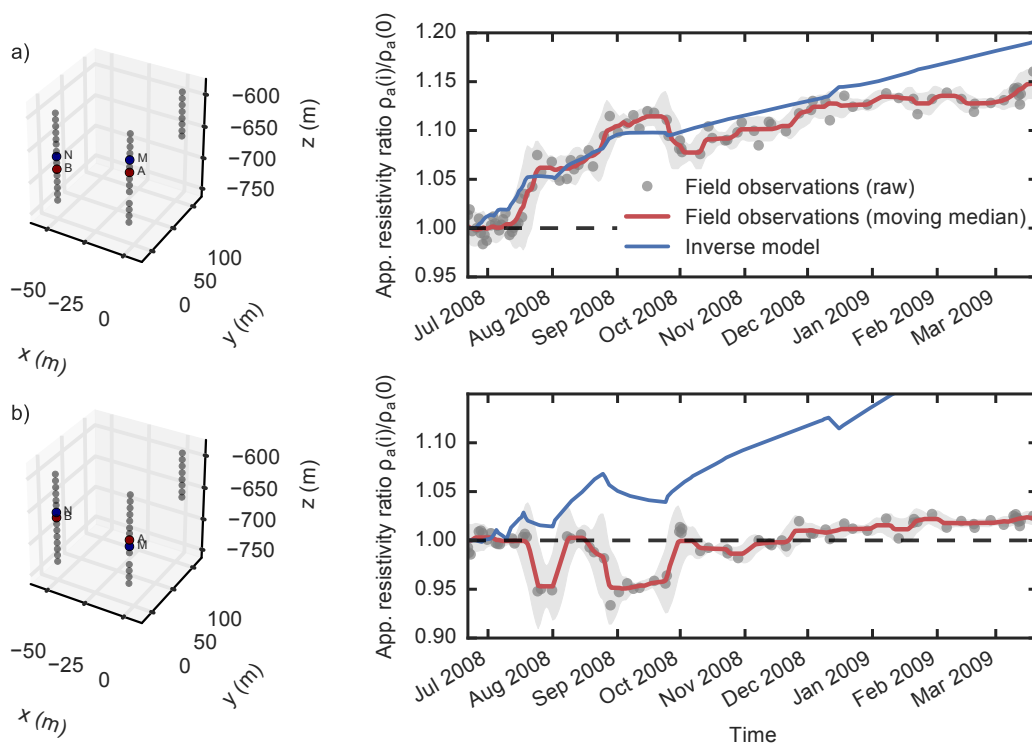
Figure 7: Geometric configurations (left-hand side) and associated measured and simulated apparent resistivity ratios over time (right-hand side) for selected configurations. Grey shaded area depicts the 2σ moving standard deviation employing a window of two weeks.
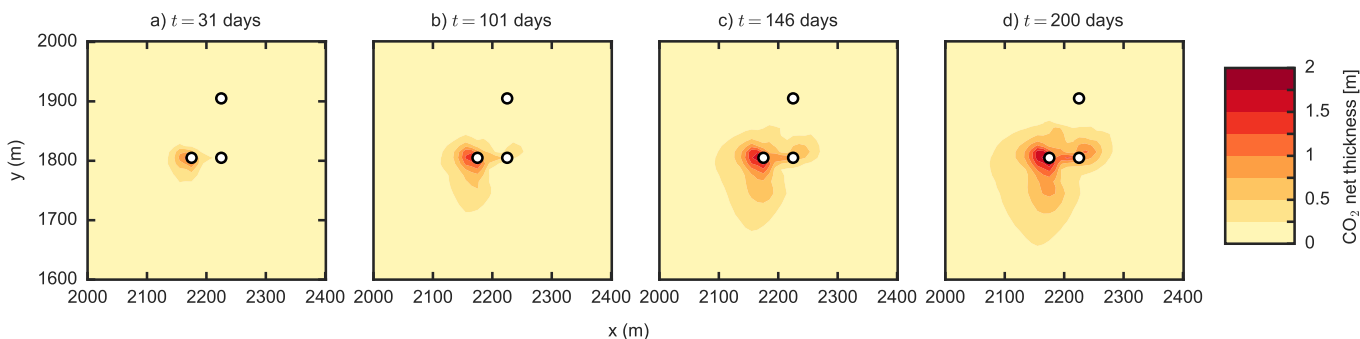
Figure 8: Modelled CO_2 migration over time. The plume thickness is vertically integrated over all reservoir layers.

crosshole ERT observations, while each time step was inverted independently in earlier ERT studies at Ketzin. The main migration direction of the CO_2 plume is predicted correctly, which is a strong indication that the calibrated permeability field is c to reality in the vicinity of the wells.

The model allows to analyse Ketzin reservoir processes in a depth not achieved before. The following field site characteristics are identified:

- The hydraulic cross hole time series between the wells Ktzi200 and Ktzi201 are identified as erroneous.

- Previous studies stated the hypothesis of a hydraulic barrier between the wells Ktzi200 and Ktzi201. The hypothesis is identified as unsubstantial as was based on the time series which are identified as erroneous.

- However, as the most barrier sensitive data are missing now, the model is so non-unique that a barrier can not be excluded.

- The permeability around the injection well is significantly reduced by salt precipitation. It corresponds to a skin factor of 10, which means that the pressure buildup is about twice as high as it would be under salt free conditions.

It is important to include all relevant information and as much datasets a possible to obtain a meaningful representation of all processes, such as the short-term pressure signal that allows to quantify the hydraulic effect of salt precipitation at Ketzin. Previous models disregard these short-term variations (Kempka and Kühn, 2013) or offer other degrees of freedom as intrinsic permeability by hydraulics is not included (Pamukcu et al., 2011; Lengler et al., 2010).

The presented approach can readily incorporate different multi-physical observation datasets. Potential candidates for extension of this framework are:

- **4D seismic data:** Inclusion of 4D seismic data could better constrain the lateral CO_2 migration compared to the exclusively well-based monitoring methods considered in this study. This could be achieved via image comparison by adding the performance criteria introduced by Lüth et al. (2015) into the objective function or alternatively, by a process-dependent seismic forward model.

- **Pulsed neutron-gamma logs:** During injection of CO_2, repeated pulsed neutron-gamma (PNG) log-

ging campaigns were carried out, which offer valuable information on saturation changes and salt precipitation (Baumann, 2013; Baumann et al., 2014). Inclusion of PNG-derived CO_2 saturation data into the presented multi-physical inversion can technically be achieved in a similar manner as inclusion of the arrival times and is expected to reduce some of the previously discussed ambiguities in ERT-based saturation estimates based on Archie's Law.

Increased confidence in the relevant processes and parameters such as permeability during CO_2 storage builds the basis for longer simulation runs and predictive assessments. We conclude that integrative, and data-driven reservoir models, such as the one presented, should be an integral part of geological CO_2 storage to improve process understanding as well as operational safety.

Acknowledgements

References

Bacci, G., Korre, A., Durucan, S., 2011. Experimental investigation into salt precipitation during co$_2$ injection in saline aquifers, pp. 4450–4456. doi:10.1016/j.egypro.2011.02.399.

Baumann, G., 2013. Determination of Displacement and Evaporation/precipitation Processes via Pulsed Neutron-Gamma (PNG) Monitoring for CO_2 Storage Operations. Ph.D. thesis. Technical University of Berlin. doi:10.14279/depositonce-3819.

Baumann, G., Henninges, J., DeLucia, M., 2014. Monitoring of saturation changes and salt precipitation during CO_2 injection using pulsed neutron-gamma logging at the Ketzin pilot site. International Journal of Greenhouse Gas Control 28, 134–146. doi:10.1016/j.ijggc.2014.06.023.

Bergmann, P., Diersch, M., Götz, J., Ivandic, M., Ivanova, A., Juhlin, C., Kummerow, J., Liebscher, A., Lüth, S., Meekes, S., Norden, B., Schmidt-Hattenberger, C., Wagner, F.M., Zhang, F., 2016. Review on geophysical monitoring of CO_2 injection at Ketzin, Germany. Journal of Petroleum Science and Engineering 139, 112–136. doi:10.1016/j.petrol.2015.12.007.

Bergmann, P., Schmidt-Hattenberger, C., Labitzke, T., Wagner, F., Just, A., Flechsig, C., Rippe, D., 2017. Fluid injection monitoring using electrical resistivity tomography - five years of co$_2$ injection at Ketzin, Germany. Geophysical Prospecting 65, 859–875. doi:10.1111/1365-2478.12426.

Bing, Z., Greenhalgh, S., 2000. Cross-hole resistivity tomography using different electrode configurations. Geophysical Prospecting 48, 887–912. doi:10.1046/j.1365-2478.2000.00220.x.

Chen, F., Wiese, B., Zhou, Q., Kowalsky, M.B., Norden, B., Kempka, T., Birkholzer, J.T., 2014. Numerical modeling of the pumping tests at the Ketzin pilot site for CO$_2$ injection: Model calibration and heterogeneity effects. International Journal of Greenhouse Gas Control 22, 200–212. doi:10.1016/j.ijggc.2014.01.003.

Class, H., Mahl, L., Ahmed, W., Norden, B., Kühn, M., Kempka, T., 2015. Matching pressure measurements and observed CO$_2$ arrival times with static and dynamic modelling at the Ketzin storage site. Energy Procedia 76, 623–632. doi:10.1016/j.egypro.2015.07.883.

Doetsch, J.A., Coscia, I., Greenhalgh, S., Linde, N., Green, A.G., Günther, T., 2010. The borehole-fluid effect in electrical resistivity imaging. Geophysics 75, F107–F114. doi:10.1190/1.3467824.

Doherty, J., Welter, D., 2010. A short exploration of structural noise. Water Resources Research 46, W05525. doi:10.1029/2009WR008377.

Fleury, M., Gautier, S., Gland, N., Boulin, P., Norden, B., Schmidt-Hattenberger, C., 2013. Advanced and integrated petrophysical characterization for CO$_2$ storage: Application to the Ketzin site. Oil & Gas Science and Technology – Revue d'IFP Energies nouvelles 68, 557–576. doi:10.2516/ogst/2012084.

Förster, A., Norden, B., Zinck-Jørgensen, K., Frykman, P., Kulenkampff, J., Spangenberg, E., Erzinger, J., Zimmer, M., Kopp, J., Borm, G., Juhlin, C., Cosma, C.G., Hurter, S., 2006. Baseline characterization of the CO$_2$SINK geological storage site at Ketzin, Germany. Environmental Geosciences 13, 145–161. doi:10.1306/eg.02080605016.

Ivandic, M., Yang, C., Lüth, S., Cosma, C., Juhlin, C., 2012. Time-lapse analysis of sparse 3D seismic data from the CO$_2$ storage pilot site at Ketzin, Germany. Journal of Applied Geophysics 84, 14–28. doi:10.1016/j.jappgeo.2012.05.010.

Jeddizahed, J., Rostami, B., 2016. Experimental investigation of injectivity alteration due to salt precipitation during CO$_2$ sequestration in saline aquifers. Advances in Water Resources 96, 23–33. doi:10.1016/j.advwatres.2016.06.014.

Kempka, T., Kühn, M., 2013. Numerical simulations of CO$_2$ arrival times and reservoir pressure coincide with observations from the Ketzin pilot site, Germany. Environmental Earth Sciences 70, 3675–3685. doi:10.1007/s12665-013-2614-6.

Kempka, T., Kühn, M., Class, H., Frykman, P., Kopp, A., Nielsen, C., Probst, P., 2010. Modelling of CO$_2$ arrival time at Ketzin - Part I. International Journal of Greenhouse Gas Control 4, 1007–1015. doi:10.1016/j.ijggc.2010.07.005.

Kempka, T., Norden, B., 2017. Inverse modelling of hydraulic testing to revise the static reservoir model of the Stuttgart formation at the Ketzin pilot site. Energy Procedia 125, 640 – 649. doi:10.1016/j.egypro.2017.08.264. european Geosciences Union General Assembly 2017, EGU Division Energy, Resources & Environment (ERE).

Köhler, S., Zemke, J., Becker, W., Wiebach, J., Liebscher, A., Möller, F., Bannach, A., 2013. Operational reservoir monitoring at the CO$_2$ pilot storage site Ketzin, Germany, in: Hou, M.Z., Xie, H., Were, P. (Eds.), Clean Energy Systems in the Subsurface: Production, Storage and Conversion. Springer Berlin Heidelberg. Springer Series in Geomechanics and Geoengineering, pp. 53–63. doi:10.1007/978-3-642-37849-2\textunderscore5.

Kummerow, J., Spangenberg, E., 2011. Experimental evaluation of the impact of the interactions of CO$_2$-SO$_2$, brine, and reservoir rock on petrophysical properties: A case study from the Ketzin test site, Germany. Geochemistry, Geophysics, Geosystems 12, Q05010. doi:10.1029/2010GC003469.

Lengler, U., Lucia, M.D., Kühn, M., 2010. The impact of heterogeneity on the distribution of CO2: Numerical simulation of CO2 storage at Ketzin. International Journal of Greenhouse Gas Control 4, 1016–1025. doi:10.1016/j.ijggc.2010.07.004.

Liebscher, A., Möller, F., Bannach, A., Köhler, S., Wiebach, J., Schmidt-Hattenberger, C., Weiner, M., Pretschner, C., Ebert, K., Zemke, J., 2013. Injection operation and operational pressure-temperature monitoring at the CO$_2$ storage pilot site Ketzin, Germany - Design, results, recommendations. International Journal of Greenhouse Gas Control 15, 163–173. doi:10.1016/j.ijggc.2013.02.019.

Lüth, S., Ivanova, A., Kempka, T., 2015. Conformity assessment of monitoring and simulation of CO$_2$ storage: A case study from the Ketzin pilot site. International Journal of Greenhouse Gas Control 42, 329–339. doi:10.1016/j.ijggc.2015.08.005.

Martens, S., Möller, F., Streibel, M., Liebscher, A., 2014. Completion of five years of safe CO$_2$ injection and transition to the post-closure phase at the Ketzin pilot site. Energy Procedia 59, 190–197. doi:10.1016/j.egypro.2014.10.366.

Norden, B., Frykman, P., 2013. Geological modelling of the triassic Stuttgart formation at the Ketzin CO$_2$ storage site, Germany. International Journal of Greenhouse Gas Control 19, 756 – 774. doi:10.1016/j.ijggc.2013.04.019.

Oliver, D.S., Chen, Y., 2010. Recent progress on reservoir history matching: a review. Computational Geosciences 15, 185–221. doi:10.1007/s10596-010-9194-2.

Pamukcu, Y., Hurter, S., Jammes, L., Vu-Hoang, D., Pekot, L., 2011. Characterizing and predicting short term performance for the In Salah Krechba field CCS joint industry project. Energy Procedia 4, 3371–3378. doi:10.1016/j.egypro.2011.02.259.

Pruess, K., Müller, N., 2009. Formation dry-out from co2 injection into saline aquifers: 1. effects of solids precipitation and their mitigation. Water Resources Research 45. doi:10.1029/2008WR007101.

Rücker, C., Günther, T., 2011. The simulation of finite ERT electrodes using the complete electrode model. Geophysics 76, F227–F238. doi:10.1190/1.3581356.

Schmidt-Hattenberger, C., Bergmann, P., Bösing, D., Labitzke, T., Möller, M., Schröder, S., Wagner, F.M., Schütt, H., 2013. Electrical resistivity tomography (ERT) for monitoring of CO$_2$ migration - from tool development to reservoir surveillance at the Ketzin pilot site. Energy Procedia 37, 4268–4275. doi:10.1016/j.egypro.2013.06.329.

Schmidt-Hattenberger, C., Bergmann, P., Kießling, D., Krüger, K., Rücker, C., Schütt, H., 2011. Application of a vertical electrical resistivity array (VERA) for monitoring CO$_2$ migration at the Ketzin site: First performance evaluation. Energy Procedia 4, 3363 – 3370. doi:10.1016/j.egypro.2011.02.258.

Schmidt-Hattenberger, C., Bergmann, P., Labitzke, T., Schröder, S., Krüger, K., Rücker, C., Schütt, H., 2012. A modular geoelectrical monitoring system as part of the surveillance concept in CO$_2$ storage projects. Energy Procedia 23, 400–407. doi:10.1016/j.egypro.2012.06.062.

Schmidt-Hattenberger, C., Bergmann, P., Labitzke, T., Wagner, F., Rippe, D., 2016. Permanent crosshole electrical resistivity tomography (ert) as an established method for the long-term co2 monitoring at the Ketzin pilot site. International Journal of Greenhouse Gas Control 52, 432 – 448. doi:10.1016/j.ijggc.2016.07.024.

Tiab, D., Donaldson, E., 2016. Petrophysics. Theory and Practice of Measuring Reservoir Rock and Fluid Transport Properties. 4 ed., Elsevier.

Wagner, F.M., Bergmann, P., Rücker, C., Wiese, B., Labitzke, T., Schmidt-Hattenberger, C., Maurer, H., 2015. Impact and mitigation of borehole related effects in permanent crosshole resistivity imaging: An example from the Ketzin CO_2 storage site. Journal of Applied Geophysics 123, 102–111. doi:10.1016/j.jappgeo.2015.10.005.

Wiese, B., Böhner, J., Enachescu, C., Würdemann, H., Zimmermann, G., 2010. Hydraulic characterisation of the Stuttgart formation at the pilot test site for CO_2 storage, Ketzin, Germany. International Journal of Greenhouse Gas Control 4, 960–971. doi:10.1016/j.ijggc.2010.06.013.

Wiese, B., Nimtz, M., Möller, F., Otto, C., Kühn, M., Liebscher, A., Schmidt-Hattenberger, C., 2012. Determination of thermodynamics in a CO_2 injection well using pressure and distributed temperature sensing. IAHS Redbook 355, 286–290.

Wiese, B., Wagner, F., Norden, B., Maurer, H., Schmidt-Hattenberger, C., 2018. Fully Coupled Inversion on a Multi-Physical Reservoir Model - Part I: Theory and Concept. International Journal of Greenhouse Gas Control 75, 262–272. doi:10.1016/j.ijggc.2018.05.013.

Zimmer, M., Erzinger, J., Kujawa, C., 2011. The gas membrane sensor (GMS): A new method for gas measurements in deep boreholes applied at the CO_2SINK site. International Journal of Greenhouse Gas Control 5, 995–1001. doi:10.1016/j.ijggc.2010.11.007.